Cost-effective monitoring of ground motion related to earthquakes, landslides, or volcanic activity by joint use of a single-frequency GPS and a MEMS accelerometer

R. Tu,[1] R. Wang,[1] M. Ge,[1] T. R. Walter,[1] M. Ramatschi,[1] C. Milkereit,[1] D. Bindi,[1] and T. Dahm[1]

Received 29 April 2013; revised 7 June 2013; accepted 10 June 2013; published 2 August 2013.

[1] Real-time detection and precise estimation of strong ground motion are crucial for rapid assessment and early warning of geohazards such as earthquakes, landslides, and volcanic activity. This challenging task can be accomplished by combining GPS and accelerometer measurements because of their complementary capabilities to resolve broadband ground motion signals. However, for implementing an operational monitoring network of such joint measurement systems, cost-effective techniques need to be developed and rigorously tested. We propose a new approach for joint processing of single-frequency GPS and MEMS (microelectromechanical systems) accelerometer data in real time. To demonstrate the performance of our method, we describe results from outdoor experiments under controlled conditions. For validation, we analyzed dual-frequency GPS data and images recorded by a video camera. The results of the different sensors agree very well, suggesting that real-time broadband information of ground motion can be provided by using single-frequency GPS and MEMS accelerometers. **Citation:** Tu, R., R. Wang, M. Ge, T. R. Walter, M. Ramatschi, C. Milkereit, D. Bindi, and T. Dahm (2013), Cost-effective monitoring of ground motion related to earthquakes, landslides, or volcanic activity by joint use of a single-frequency GPS and a MEMS accelerometer, *Geophys. Res. Lett.*, *40*, 3825–3829, doi:10.1002/grl.50653.

1. Introduction

[2] Displacements associated with earthquakes and volcanic activity may span multiple scales, from submillimeters per year to meters within seconds [*Dzurisin*, 2007; *Segall*, 2010]. The motion of landslides and glaciers can show similar multiscale characteristics. Rapid detection and quantification of this multitude of displacement scales is challenging and commonly approached by combining various technical concepts. However, many of these displacements may involve accelerations on the order of 10^{-5} to 10 m/s^2. For technical reasons, the scales of deformation are often not fully detected, and the associated processes remain poorly understood.

[3] In recent years, high-rate GPS technology has improved and is increasingly useful for exploring large displacements and accelerations [*Bilich et al*., 2008; *Larson*, 2009; *Blewitt et al*., 2009]. However, a well-known limitation of high-rate GPS is that its high precision can only be guaranteed in the low-frequency band. For frequencies larger than a few hertz, GPS data generally involve large uncertainties caused by instrumental noise [*Genrich and Bock*, 2006]. By comparison, digital accelerometers can measure the strong ground shaking with a much higher resolution than the GPS, but their records usually include so-called baseline errors, which are induced dominantly by ground tilting. Though these errors are generally very small, they affect seismometer records in the low-frequency band and thus prevent retrieving the true ground velocity and displacement from the recorded accelerograms [*Boore*, 2001; *Wang et al*., 2011]. In previous studies, baseline errors of accelerometer sensors were corrected using empirical methods, which generally involve uncertainties that are not easily quantified without a geodetic reference [*Wang et al*., 2011].

[4] Many authors have suggested an integrated analysis of high-rate GPS and accelerometer data [*Emore et al*., 2007; *Bock et al*., 2011; *Wang et al*., 2013]. In most cases, the displacement data from a nearby GPS station are used as the reference to optimize the empirical baseline correction of the accelerometer records. To improve cost-effectiveness of colocated devices, we propose a different approach for the integrated analysis. In this approach, the site velocity is estimated using carrier phase observations of a single-frequency GPS receiver with satellite orbits and clocks from the broadcast navigation information that is decoded from the received satellite signals [*Colosimo et al*., 2011]. Therefore, it can be performed station by station and has good timeliness. In general, most errors, such as atmospheric delays and biases in the satellite orbits and clocks, can be significantly reduced by using epoch-differentiated observations [*Colosimo et al*., 2011]. However, the remaining atmospheric errors, satellite clock and orbit biases, multipath effects, and high-frequency noises are still noticeable. Such remaining errors result not only in high-frequency noises but also in a slow trend in the estimated velocity time series.

[5] In this paper, we propose a new approach to integrate measurements from a single-frequency GPS and a MEMS (microelectromechanical systems) accelerometer. Both of these sensors are relatively cheap, currently available for a few hundred dollars only, which harshly contrasts to Global Navigation Satellite Systems or seismic stations that are available at prices approximately 20–50 times higher. Based on the validated results from outdoor experiments, we demonstrate how our approach benefits from the complementary capabilities of the combined system to provide broadband ground motion information.

[1]GFZ German Research Centre for Geosciences, Potsdam, Germany.

Corresponding author: R. Wang, GFZ German Research Centre for Geosciences, DE-14473 Potsdam, Germany. (wang@gfz-potsdam.de)

0094-8276/13/10.1002/grl.50653

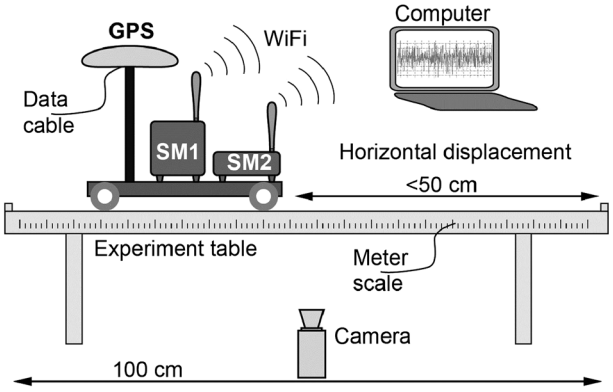

Figure 1. A sketch of the sledge experiment, including a GPS receiver, a video camera, a low-cost MEMS accelerometer (SM1), and a high-precision Guralp accelerometer (SM2).

2. Method

[6] Cost-effective sensors are appropriate for monitoring strong ground motion events. Earthquakes, for instance, can be easily detected by the measured ground acceleration exceeding a certain threshold. In practice, it is usually more difficult to estimate the end of a ground motion event (such as an earthquake) because of coda waves that may decay slowly but without producing any permanent ground deformation. We propose to consider that a ground motion event is over when the ground acceleration has decreased below 10% of its peak ground acceleration for a long enough time (e.g., as long as the pre-event time window).

[7] Once a ground motion event is detected, the joint data processing is performed in three steps. First, an appropriate pre-event time window (10–20 s) is chosen. Within the pre-event window, the ground motion is considered negligible. Thus, the initial trend in the GPS and the initial offset in the accelerometer baseline can be determined independently and will be removed from their respective data streams. Second, the trend-corrected GPS velocity is integrated into the GPS-based displacement, which provides the reference for the accelerometer-based displacement, so that the baseline shift in the accelerometer record can be derived by comparing the two displacement data sets. Finally, time series of displacement, velocity, and acceleration are derived from the baseline-corrected accelerometer record. Such broadband ground motion information is particularly important for characterizing the event source.

[8] Define V_G as the real-time GPS velocity estimation based on the broadcast ephemeris and epoch difference measurement [*Colosimo et al.*, 2011] since an initial time $t = 0$, prior to the detected event start, denoted as t_0. Through a linear regression within the pre-event time window $[0,t_0]$, we can estimate the initial trend in V_G given by $\alpha_0+\beta_0 t$ and extrapolate it to the whole event period. After correcting for this initial trend, we calculate the GPS-based displacement time history by integration,

$$U_G(t) = \int_0^t [V_G(\tau) - (\alpha_0 + \beta_0\tau)]d\tau. \quad (1)$$

[9] On the other hand, we obtain the accelerometer-based displacement time history by double integration of the accelerometer records, defined as A_S,

$$U_S(t) = \int_0^t \int_0^\tau [A_S(\xi) - A_0]d\xi d\tau, \quad (2)$$

where A_0 represents the pre-event baseline offset of the accelerometer sensor.

[10] Recognizing the complementary advantage of the two measuring instruments, we may suppose that the time series $U_G(t)$ and $U_S(t)$ can be expressed in the form

$$U_G(t) = u(t) + G_{\text{noise}}(t) \quad (3)$$

and

$$U_S(t) = u(t) + S_{\text{trend}}(t), \quad (4)$$

where u is the true ground displacement, G_{noise} represents the high-frequency noise included in the GPS-based displacement data, and S_{trend} represents the low-frequency trend in the accelerometer-based displacement data caused by the event-induced baseline errors.

[11] Without using the GPS data, S_{trend} has to be estimated empirically. To use the GPS and accelerometer data jointly, we introduce a residual time series between U_S and U_G,

$$U_{\text{dif}}(t) = U_S(t) - U_G(t) = S_{\text{trend}}(t) - G_{\text{noise}}(t), \quad (5)$$

so that S_{trend} and G_{noise} can be estimated by the low-pass and high-pass filters applied to U_{dif}, respectively. In our approach, we determine S_{trend} by smoothing U_{dif} through a moving Gaussian window with a bandwidth of 1–2 s and then the actual displacement time series u can be estimated by subtracting S_{trend} from U_S,

$$u(t) = U_S(t) - S_{\text{trend}}(t). \quad (6)$$

[12] As S_{trend} can be interpolated and even extrapolated for a short time, the time series u of the accelerometer sampling rate can be achieved, although the trend can only be estimated using the GPS and accelerometer data at the common epochs. The true ground velocity and acceleration are obtained by differentiating u over time.

[13] In order to validate the low-cost combination, dual-frequency GPS and camera video data were analyzed through postprocessing, as described in the next section.

3. Outdoor Experiments

[14] Figure 1 shows the sledge that we used in several outdoor experiments carried out in December 2012. The sledge, which can move along a table, includes a dynamic GPS antenna, a low-cost MEMS accelerometer [*Fleming et al.*, 2009], and a high-precision accelerometer (CMG-5T Compact made by Guralp Systems Ltd.). The sampling rates are 50 Hz for the GPS and 100 Hz for the two accelerometer sensors. The maximum sliding distance of the sledge was restricted to about 0.5 m in one direction. A video camera recorded the sledge motion from a distance of 10 m at 25 fps (frames per second). The images, with a constant pixel resolution of 3 mm, were analyzed by manual identification of the sledge and automatic image-to-image tracking using a normalized cross-correlation code [*Walter*, 2011].

[15] We use the aforementioned joint data processing approach in simulated real-time mode for the single-frequency (L1) GPS data and accelerometer records. For illustration purposes, we show a selected experiment, in

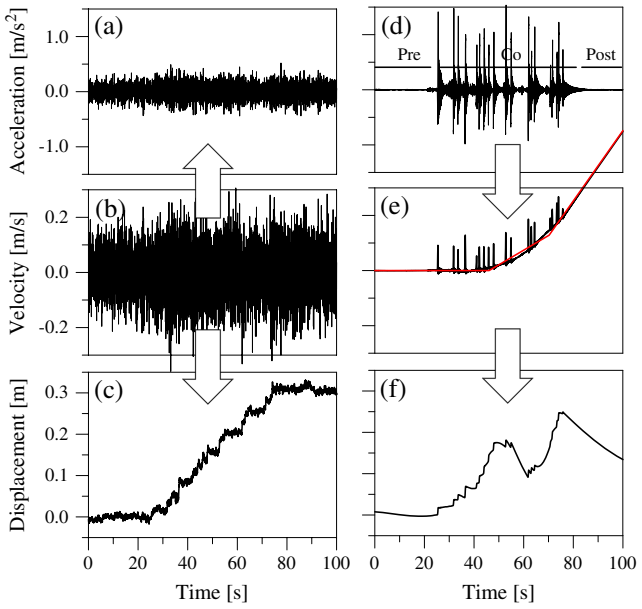

Figure 2. Sledge acceleration, velocity, and displacement based on the (a–c) single-frequency GPS and (d–f) MEMS accelerometer data. The original velocity estimates derived from the GPS carrier observations and the raw data of the MEMS accelerometer are plotted in Figures 2b and 2d, respectively. The bilinear red curve in Figure 2e represents the empirical correction of the event-induced trend in the accelerometer-based velocity time series.

which the sledge is shifted stepwise from 0 to 0.3 m. Results of other experiments are summarized at the end of this section. Figure 2 shows the sledge velocity obtained from the single-frequency GPS carrier observation and the acceleration from the MEMS accelerometer records. For simplicity, the pre-event trend in the GPS velocity time series and the initial offset in the accelerometer records have been removed. To show the complementary information involved in the two different measurements, all differentiated and integrated time series are given in Figure 2 as well.

[16] Although the GPS velocity data and the derived acceleration seem noisy, the integrated displacements reflect an uncertainty of a few centimeters, compared with the dual-frequency GPS and camera results (Figure 3c) as reference. In contrast, the original accelerometer-based acceleration and velocity (after the empirical baseline correction) have a much higher signal-to-noise ratio. From the postevent trend of the accelerometer-based velocity data (Figure 2e), we can derive the permanent baseline shift of the accelerometer sensor to be 0.004 m/s^2, which can be explained by a tilt of 0.024° of the sledge after the experiment, causing the gravity to be projected in the horizontal direction (0.004 m/s^2 ≈ 9.8 m/s^2 × sin 0.024°). Though this baseline shift accounts for only ~0.1% of the peak acceleration, it is impossible to obtain the displacement through double integration of the original accelerometer record. The displacement time history shown in Figure 2f is calculated by using the empirical baseline correction suggested by *Wang et al.* [2011]. This time series clearly exhibits two kinks resulting from the bilinear approximation used for the baseline correction.

[17] For the combined data processing, the lower sampling rate of the two measurement systems, which is 50 Hz in this case, is used for estimating the trends. Figure 3a shows that the residual time series U_{dif} dominates the rapid trend in the accelerometer-based displacement time series. Subtracting the smoothed U_{dif}, which we obtained by using a moving Gaussian window of 2 s (i.e., 100 epochs), from the accelerometer-based displacement U_S (the black curve in Figure 2f), we estimate the displacement and velocity time series shown in Figures 3b and 3c, respectively. Particularly, Figure 3b shows that the stepwise sliding signals of the experimental sledge have been clearly resolved with a bias less than 2–3 cm using the real-time combined data processing approach, validated by the camera (25 Hz) measurements and the results of the dual-frequency GPS obtained using the precise point positioning approach through postprocessing [*Kouba*, 2003]. In Figure 3c, the velocity time series derived from camera images is also shown, and its amplitude appears systematically larger than that from the low-cost combination. One may explain this discrepancy by the limited pixel resolution of the camera (~0.1 cm), the stabilizer, and the used JPEG compression coded in blocks of 8 × 8 pixels, leading to initial detection inertia and, consequently, an overestimate of the velocity peaks. Notice that the camera-based velocity also shows stochastic noise on the same order of the overestimate. The displacement values were not affected by this data reduction.

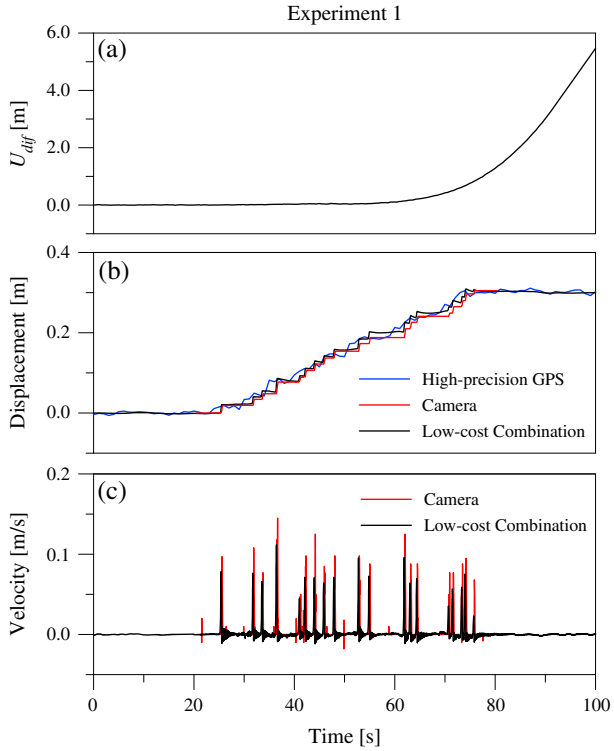

Figure 3. Results from the combined processing of the GPS and accelerometer data for the selected experiment. (a) Residual time series U_{dif} between the accelerometer- and GPS-based displacement time series. (b) Displacement time series u retrieved by subtracting the smoothed U_{dif} from the accelerometer-based displacement, validated by the dual-frequency GPS (blue) and camera results (red). (c) Velocity time series $v = \mathrm{d}u/\mathrm{d}t$, compared with the camera observations.

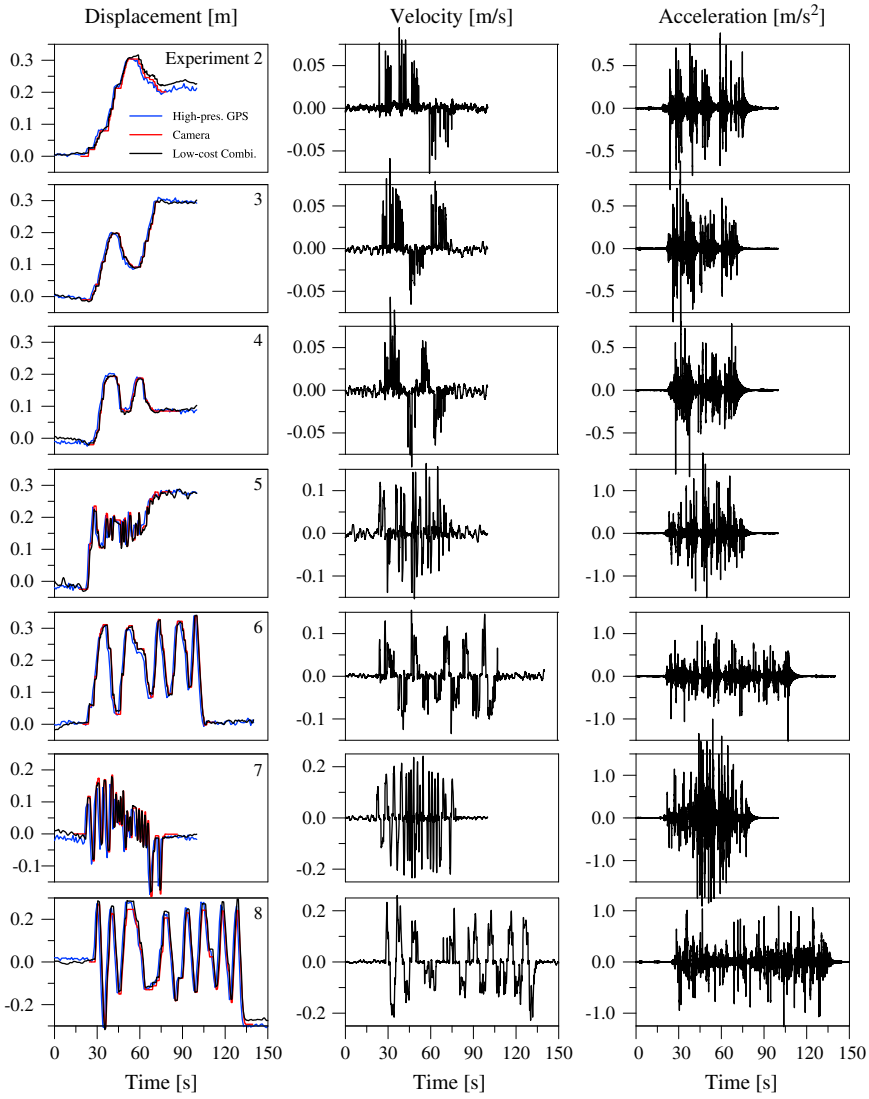

Figure 4. Results from the other seven experiments. (left) Displacement time series retrieved using the combined processing of the GPS and accelerometer data, validated by the results from the dual-frequency GPS (blue) and camera observations (red). (middle) Velocity time series obtained by differentiating the corresponding displacement time series. (right) Acceleration time series given by the records of SM1.

[18] In Figure 4, we summarize the results from the combined data processing for the other seven outdoor experiments. For each experiment, the postevent part of the combined GPS and accelerometer data is used to evaluate the uncertainty of the low-cost measurement system. In all experiments, the displacement deviations of the combined system are within 2–3 cm, using the dual-frequency GPS and camera results as reference. Note that we also tested the proposed procedure using the records by the Guralp sensor instead of the MEMS sensor but found no substantial difference in the retrieved velocity and acceleration time series. This observation verifies the finding by *Picozzi et al.* [2011] that for frequencies over 0.5 Hz, there is no significant difference between the response spectra between the MEMS and Guralp sensors that we used in this study.

4. Discussion and Conclusions

[19] We have proposed and tested a simple, but sophisticated, approach to integrate colocated high-rate GPS and accelerometer measurements. Based on our outdoor experiments, the real-time accuracy of the combined system for the horizontal displacement is on the order of 2–3 cm, validated by the dual-frequency GPS and camera observations.

[20] Note that when processing a ground motion event, the same broadcast ephemeris record has to be used during the whole event period to avoid possible jumps in the results due to the discontinuity of adjacent ephemeris records. Additionally, notice that we have combined the two measurements in the displacement domain. In principle, the combination should also work in the velocity domain. However, the basic idea of our approach is to estimate the low-frequency trend in the residual data between the accelerometer- and GPS-based time series. Such trend becomes amplified through integrations and therefore can be better determined in the displacement domain than in the velocity domain. Another issue to be addressed is the choice of the low-pass filter used to separate the accelerometer-based trend from the GPS-based noise. We have used a Gaussian smoothing window, which corresponds to an acausal low-pass filter

because it covers the same length (1 s or 50 epochs) of past and future data. Due to the 1 s time delay, the tool that we have presented here is, strictly speaking, applicable for the near-real-time joint data processing.

[21] In summary, our experimental results have shown that the combined system of a single-frequency GPS and a MEMS accelerometer is able to monitor broadband ground motion associated with strong acceleration events with precision satisfying most current demands in real-time seismology and earthquake engineering, with potential applications in other fields as well. To solve the long-term monitoring problem, however, the dual-frequency GPS and broadband seismometer are still required and cannot be replaced by such low-cost system. Considering the cost of telemetry, the low-cost system is suitable not only for implementing local dense networks to monitor active tectonic faults and volcanos but also for collocating with existing geodetic and seismic instruments.

[22] **Acknowledgments.** This paper was partly funded by the REAKT project (Towards Real-Time Earthquake Risk Reduction) of the European Seventh Framework Program (grant agreement 282862). R. Tu was supported by the China Scholarship Council. Álvaro González and Robert A. Clements proofread the manuscript. We thank S. Stein and other two anonymous reviewers for their valuable comments.

[23] The Editor thanks Seth Stein and two anonymous reviewers for their assistance in evaluating this paper.

References

Bilich, A., J. F. Cassidy, and K. M. Larson (2008), GPS seismology: Application to the 2002 Mw 7.9 Denali Fault earthquake, *Bull. Seismol. Soc. Am.*, *98*, 593–606.

Blewitt, G., W. C. Hammond, C. Kreemer, H. P. Plag, S. Stein, and E. Okal (2009), GPS for real-time earthquake source determination and tsunami warning systems, *J. Geod.*, *83*, 335–343.

Bock, Y., D. Melgar, and B. W. Crowell (2011), Real-time strong-motion broadband displacements from collocated GPS and accelerometers, *Bull. Seismol. Soc. Am.*, *101*, 2904–2925.

Boore, D. M. (2001), Effect of baseline corrections on displacement and response spectra for several recordings of the 1999 Chi-Chi, Taiwan, earthquake, *Bull. Seismol. Soc. Am.*, *91*, 1199–1211.

Colosimo, G., M. Crespi, and A. Mazzoni (2011), Real-time GPS seismology with a stand-alone receiver: A preliminary feasibility demonstration, *J. Geophys. Res.*, *116*, B11302, doi:10.1029/2010JB007941.

Dzurisin, D. (2007), *Volcano Deformation: Geodetic Monitoring Techniques*, Praxis, Chichester, U. K., pp. 441.

Emore, G. L., J. S. Haase, K. Choi, K. M. Larson, and A. Yamagiwa (2007), Recovering seismic displacements through combined use of 1-Hz GPS and strong-motion accelerometers, *Bull. Seismol. Soc. Am.*, *97*, 357–378.

Fleming, K., M. Picozzi, C. Milkereit, F. Kuehnlenz, B. Lichtblau, J. Fischer, C. Zulfikar, O. Ozel, and the SAFER and EDIM working groups (2009), The Self-Organising Seismic Early Warning Information System (SOSEWIN), *Seismol. Res. Lett.*, *80*, 755–771.

Genrich, J. F., and Y. Bock (2006), Instantaneous geodetic positioning with 10–50 Hz GPS measurements: Noise characteristics and implications for monitoring networks, *J. Geophys. Res.*, *111*, B03403, doi:10.1029/2005JB003617.

Kouba, J. (2003), Measuring seismic waves induced by large earthquakes with GPS, *Stud. Geophys. Geod.*, *47*, 741–755.

Larson, K. M. (2009), GPS seismology, *J. Geod.*, *83*, 227–233.

Picozzi, M., S. Parolai, M. Mucciarelli, C. Milkereit, D. Bindi, R. Ditommaso, M. Vona, M. R. Gallipoli, and J. Zschau (2011), Interferometric analysis of strong ground motion for structural health monitoring: The example of the L'Aquila, Italy, seismic sequence of 2009, *Bull. Seismol. Soc. Am.*, *101*, 635–651, doi:10.1785/0120100070.

Segall, P. (2010), *Earthquake and Volcano Deformation*, Princeton Univ. Press, Princeton, U. K.

Walter, T. R. (2011), Low cost volcano deformation monitoring: Optical strain measurements and application to Mount St. Helens data, *Geophys. J. Int.*, *186*(2), 699–705, doi:10.1111/j.1365'-246X.2011.05051.x.

Wang, R., B. Schurr, C. Milkereit, Z. Shao, and M. Jin (2011), An improved automatic scheme for empirical baseline correction of digital strong-motion records, *Bull. Seismol. Soc. Am.*, *101*, 2029–2044.

Wang, R., S. Parolai, M. Ge, M. P. Jin, T. R. Walter, and J. Zschau (2013), The 2011 Mw 9.0 Tohoku earthquake: Comparison of GPS and strong-motion data, *Bull. Seismol. Soc. Am.*, *103*(2B), 1336–1347, doi:10.1785/0120110264.